Friction Stir Processing (FSP) of Multiwall Carbon Nanotubes and Boron Carbide Reinforced Aluminum Alloy (Al 5083) Composites

Mahmood Khan, Wilayat Husain Syed, Shahid Akhtar and Ragnhild E. Aune

Abstract Friction Stir Processing (FSP) is a novel solid-state processing technique for fabrication of high strength surface composites. In present study, FSP was used to compare the cold formability of individually reinforced, hybrid and reference FSP samples of aluminum alloy Al5083. A plate of alloy containing MultiWall Carbon NanoTubes (MWCNTs) and boron carbide particles (B_4C) was processed by FSP and characterized. FSP composite containing MWCNTs was found to fracture during the bend-ductility test, while boron carbide particles reinforced FSP composites had superior cold bending formability along with the reference FSP sample. Cracking was also observed in hybrid FSP composite samples in lesser extent as compared to individually reinforced MWCNTs FSP composite. Possible cause of failure was identified as clustering of MWCNTs and weak interfacial bonding with the aluminum alloy matrix. Detailed metallographic and mechanical testing investigations revealed that the distribution of reinforcement at nanoscale and single pass processing played a vital role in generating defects and sinking of reinforcement particles in Al5083 matrix.

Keywords Friction Stir Processing (FSP) · MWCNTs · B_4C · Aluminum composite

M. Khan (✉) · W. H. Syed
Department of Materials Science and Engineering, Institute of Space Technology, Islamabad, Pakistan
e-mail: mahmood.khan@ntnu.no; mahmoodkhan77@gmail.com

W. H. Syed
e-mail: wilayat.hussain@ist.edu.pk

M. Khan · R. E. Aune
Department of Materials Science and Engineering, Norwegian University of Science and Technology (NTNU), Trondheim, Norway
e-mail: ragnhild.aune@ntnu.no

S. Akhtar
Norsk Hydro, Karmåy Primary Production, Håvik, Norway
e-mail: shahid.akhtar@hydro.com

Introduction

FSP is a method of changing the properties of a metal through intense, localized plastic deformation, and it is a modification of friction stir welding used to produce solid-state composites. Through FSP the microstructure of the processed surface is modified under action of a rotating tool by a mechanically induced sliding motion [1], and it is the movement/action of the tool that normally results in frictional heat and severe plastic deformation. Microstructural modification subsequently affects the mechanical properties of the base metal, i.e. hardness, tensile and compression strength [2]. Strength is often among the properties reported in literature [3] to have been improved by FSP as a result of elimination of microstructural defects like cracking and porosity. This makes friction stirred processed material more stress resistant [4].

Different types and morphologies of reinforcements have been incorporated by FSP in base metals such as aluminum oxide, silicon carbide, boron carbide, MWC-NTs, etc. to prepare surface composites. In the case of aluminum and its alloys, range of particles from nanometer [5] to micrometer [6] have been reported to be incorporated by FSP, i.e. silicon carbide [7], aluminum oxide [8], boron carbide [9] and cerium oxide [10] are among the carbonaceous nanoreinforcements incorporated [11] as well as carbon nanotubes [5] and graphene nanoplatelets [12]. The combination of two chemically and morphologically dissimilar reinforcements has been less explored from the perspective of dispersion and effect of processing parameters of FSP.

Most of the studies on FSP reported in literature have focused on tooling and processing parameters along with general trend of improvement in mechanical properties of the resulting composites. Formability of the FSP composite in comparison with a nano and micro combination of reinforcements has, however, rarely been explored. Based on this, the present study focuses on the use of FSP to develop surface composites of Al5083 containing MWCNTs and B_4C particles. The B_4C particles, which are ceramic particles, possess high hardness [13] along with the MWCNTs which have exceptionally high strength and stiffness [14]. The baseline data for the hybrid composites was obtained by preparing FSP samples without the addition of any reinforcements. Microstructural observation and reinforcement distribution were examined by optical and scanning electron microscope. Micro Vickers hardness, tensile test and bending tests were carried out to characterize the mechanical performance. Finally, the results are critically reviewed in the light of available related data in literature.

Table 1 Aluminum alloy 5083 chemical composition obtained from X-ray fluorescence examination

Element	Mg	Fe	Mn	Cu	Si	Cr	Zn	Other	Al
wt%	4–4.9	≥0.4	0.4–1	≥0.1	0–0.4	0.05–0.25	0–0.1	0–0.05	Balance

Fig. 1 SEM images of reinforcements using **a** B_4C particles, **b** Multiwall CNTs, and **c** particle size test results of B_4C particles
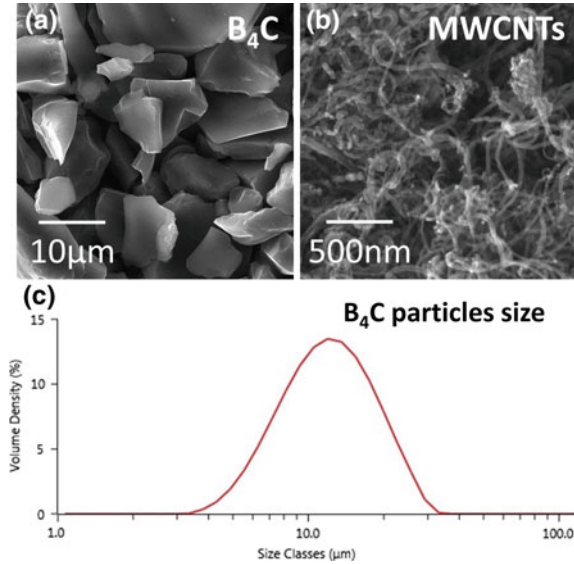
Experimental

Materials

Commercially rolled plate of Al5083, 6 mm thick was used with nominal composition shown in Table 1. 10 μm sized B_4C particles as shown in Fig. 1a, c, and MWCNTs with average length and diameter of 1–2 μm and 10–20 nm, respectively, were procured from Hongwu International Group, China, see Fig. 1b. H-13 tool steel with a diameter of 16 mm and 4.5–6.0 mm conical pin was used as a tool. A taper angle of 5° was made for the conical pin with a length of 4.5 mm (Fig. 2).

Manufacturing

Holes were drilled in the base plate of Al5083 with a diameter of 2.0 mm and a depth of 3.0 mm. SI-3 M drilling machine (Siddhapura Enterprise, India) was used to drill holes ~10 mm apart. Each hole was filled with MWCNTs or B_4C particles, followed by manual compaction using a 1.8 mm diameter flat bottom face tool. Mixture of
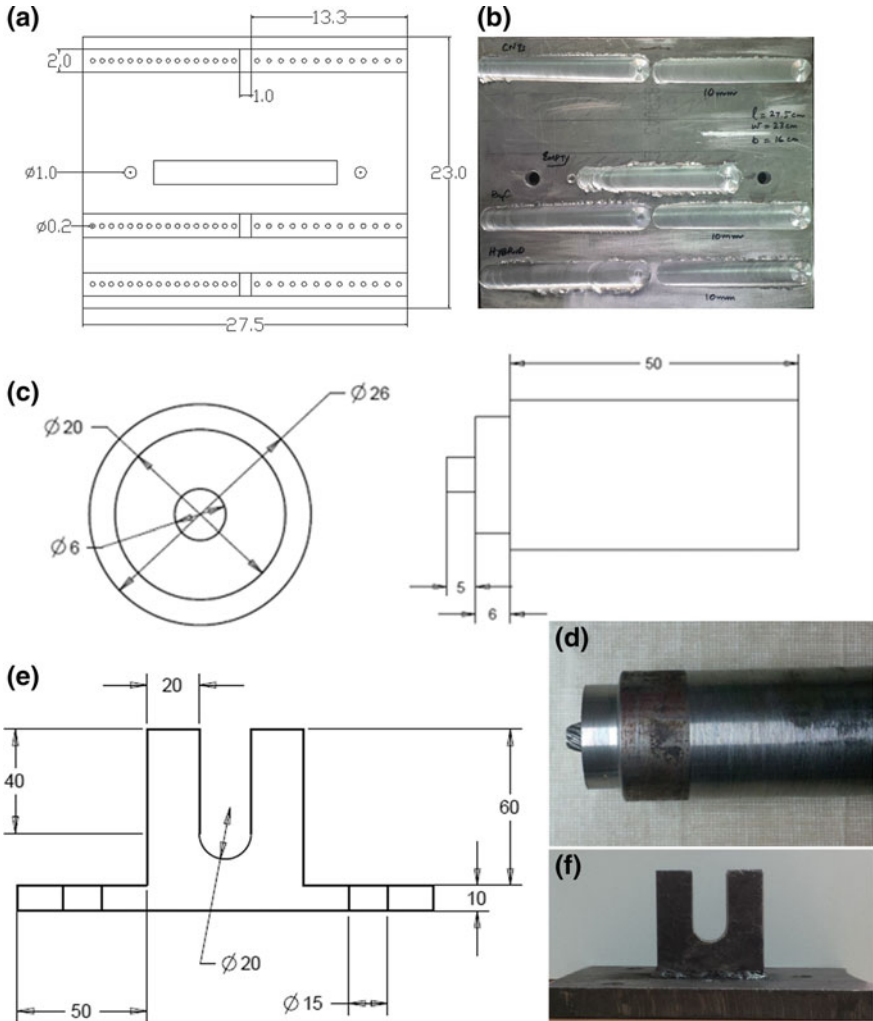
Fig. 2 Drawings and images of **a** Al5083 plate dimension, **b** Al5083 plate after FSP, **c** drawing H-13 tool, **d** image of FSP tool after machining [15], **e** customize bend-ductility die, and **f** Die after fabrication

equal weights of B$_4$C and MWCNTs were mixed at 100 rpm in ball mill for 30 min to prepare hybrid mixtures. In Fig. 3, schematics of FSP process and bend-ductility test is presented. Single pass FSP at rotational speed of 750 rpm, traverse speed of 16 mm/min, and tilt angle of 2 was selected for milling operation on LK5 N milling machine (Pakistan Machine Tool Factory).
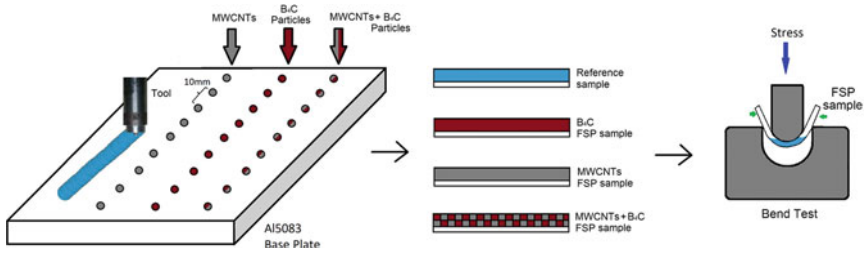
Fig. 3 Schematics of the FSP process showing reference and composite samples used for bend-ductility tests

Characterization

Radiography was performed on all FSP samples for detection of any major internal defects due to processing, using Andrex Smart X-ray machine (225 kV, 88527, Denmark). Macroscopic images were collected from stereoscope (3M05766, Olympus SZX7, Japan), and microstructure examinations was carried out using IMM 901 microscope (Metkon Instruments, Turkey). The metallographic study was carried out on mirror like surfaces after etching and polishing using a Keller's reagent (3 ml HCl, 2 ml HF, 5 ml HNO_3 and 150 ml distilled water). Scanning Electron Microscope (SEM) was also used to examine the fractured surfaces, using a MIRA-III (TESCAN, Czech Republic) in secondary electron imaging mode.

Hardness testing was carried out according to the standard ASTM E-384 on 550 g test load with 5 s dwell time, using Karl Frank microhardness tester. A hardness profile was made from the cross section of each FSP sample, and later used to record the variations from the FSP tool leading and trailing end. For tensile testing, sample were cut across the FSP area so as to allow for testing of FSP area specifically in the gauge length of the specimen. Four samples of each FSP combination were tested with a dimension of 25 mm in length, 2 mm in thickness, and 5 mm in width. Bend-ductility tests were performed using a custom made U-shaped die, see Fig. 2e, f, under guidelines of the ASTM E-190 standard. Convex surfaces of the bend FSP samples were examined; firstly with the naked eyes then using a stereoscope for fractured surfaces.

Results and Discussion

Radiography

Figure 4, shows radiographs of the FSP sample and composites. Excessive beads formed on sample surface, due to tool forward and rotating motion were removed with a tool to avoid perky ripples in radiographs of the FSP composites. The green
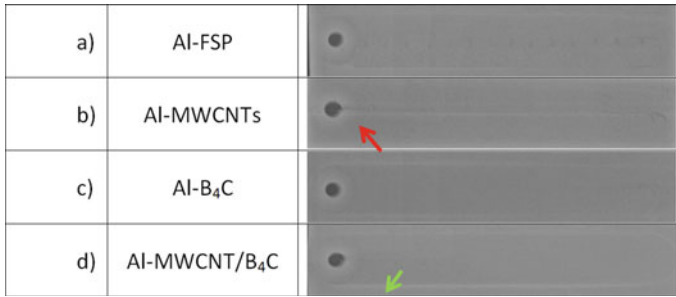
Fig. 4 Radiograph images of **a** Reference Al5083 sample, **b** Al-MWCNTs composite sample, **c** the Al-B$_4$C composite sample and **d** the Al-MWCNT/B$_4$C composite sample

arrow in Fig. 4d shows an example of such a bright line at the edge of the FSP area. No defects in the radiography were detected in any other FSP samples, see Fig. 4a, c and d. A short dark line can however be seen in Fig. 4b representing the Al-MWCNTs FSP composite, see red arrow. It is a well-known fact that in radiography, loss of material can often be seen as a dark area/zone due to the lack of fusion in this specific area. Lack of fusion originates from microstructure under the influence of (1) type of reinforcement used and (2) distribution of reinforcement present in the matrix. No dark lines similar to the line seen in Fig. 4b was observed in the plain FSP, B$_4$C and hybrid FSP composites. Presence of MWCNTs in Al-MWCNTs FSP sample did, however, have an effect on the macrostructure. The lack of fusion can in other words be related to single pas FSP processing which is process parameter.

Microstructure

In Fig. 5, micrographs of the cross section of FSP samples are presented. As can be seen from the figure, three distinct areas/zones can be seen, i.e. the base metal (BM) zone where as received Al5083 rolled structure is present, the stir zone (SZ) zone which is in direct influence of the FSP tool and a Thermomechanically Affected Zone (TMAZ). Predominantly the affected areas/zones have the same dimensions as the tool pin, except for a fractional spread due to the rotation of conical threaded pin. No visible discontinuity can be observed in the bare reinforcement FSP samples, see Fig. 5a. The Al-MWCNTs composites showed, however, a distinct type of defect, see Fig. 5b that is believed to originate from stirring action of the tool and lack of compensation for the base metal to fill the drilled holes cavity filled with MWCNTs. The FSP composite with B$_4$C showed darker shades related to the distribution of microsized reinforcement, but no other defects, see Fig. 5c. The hybrid FSP composites, Al-MWCNT/B$_4$C, showed no defects, see Fig. 5d. It is believed that the ceramic B$_4$C reinforcement lowered the defect intensity by compensating the loss of material by effectively filling the empty volume of the drilled holes.
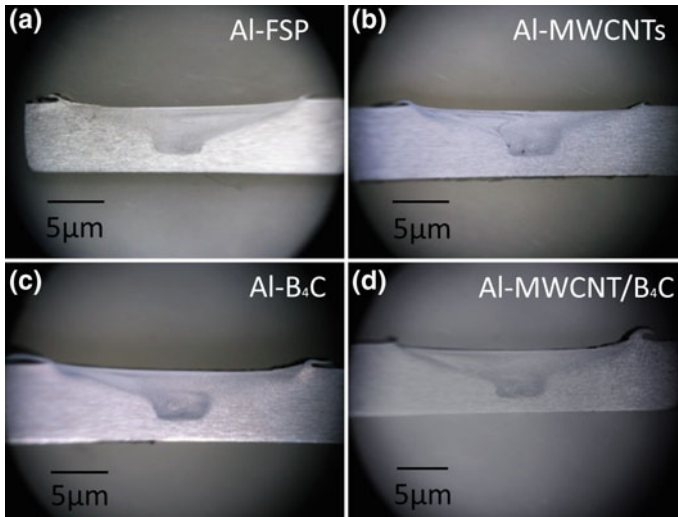
Fig. 5 Cross-sectional stereoscopic images of **a** reference Al5083 sample, **b** Al-MWCNTs composite sample, **c** the Al-B$_4$C composite sample, and **d** the Al-MWCNT/B$_4$C composite sample

FSP processing is usually characterized by using tool traversing zones. In Fig. 6 optical images of the reference FSP sample and composites are presented. The cross section views of the microstructures are identified by leading and trailing sides of SZ zone in all the FSP samples, see Fig. 6a. Grain size and morphological changes has been reported in an earlier study by McNelley et al. [16], confirming as rolled lamellar grains of the base plate Al5083 modified due to tool stirring action. As severe plastic deformation takes place the finer grains emerge, see Fig. 6b. This behavior is in good agreement with the findings of Lee et al. [17], who investigated the effect of MWCNTs on tensile properties of FSP composite. Presence of Heat- Affected Zone (HAZ) have also been reported in a study by Taban and Kaluc [18] where they proposed that HAZ usually exists between stirred, TMAZ regions and BM zones. In the present study grain coursing was not observed, and as a result nor was HAZ. In Fig. 6c the microstructure of Al-MWCNTs sample is presented. As can be seen from the figure, prominently dark lines of MWCNTs clusters exist, visible at TMAZ regions between BM and SZ zones. Compared to the Al-B$_4$C composite, see Fig. 6d, the appearance of the SZ and BM zones clearly differentiates from the FSP composite with MWCNTs. As low free volume was present in the micrometer size B$_4$C particle reinforced composites used to fill in the drill holes, thus better distribution of the reinforcement at single pass was observed as compared to nanoreinforcement, i.e. MWCNTs. The B$_4$C particles were found mainly trapped in the TMAZ region. The hybrid FSP composite Al-MWCNT/B$_4$C was observed to be dominated by the B$_4$C dispersion trend, see Fig. 6e. Lack of MWCNT-clustering in the TMAZ region is believed to be due to presence of B$_4$C particles in the TMAZ region with thinner

Fig. 6 Optical
microstructures of FSP
reference and composite
sample's cross sections,
showing tool's leading and
trailing edges of FSP zones;
a reference sample, **b** high
magnification SZ and BZ
zones, **c** Al-MWCNTs
sample, **d** Al-B$_4$C sample,
and **e** Al-MWCNT/B$_4$C
sample [15]
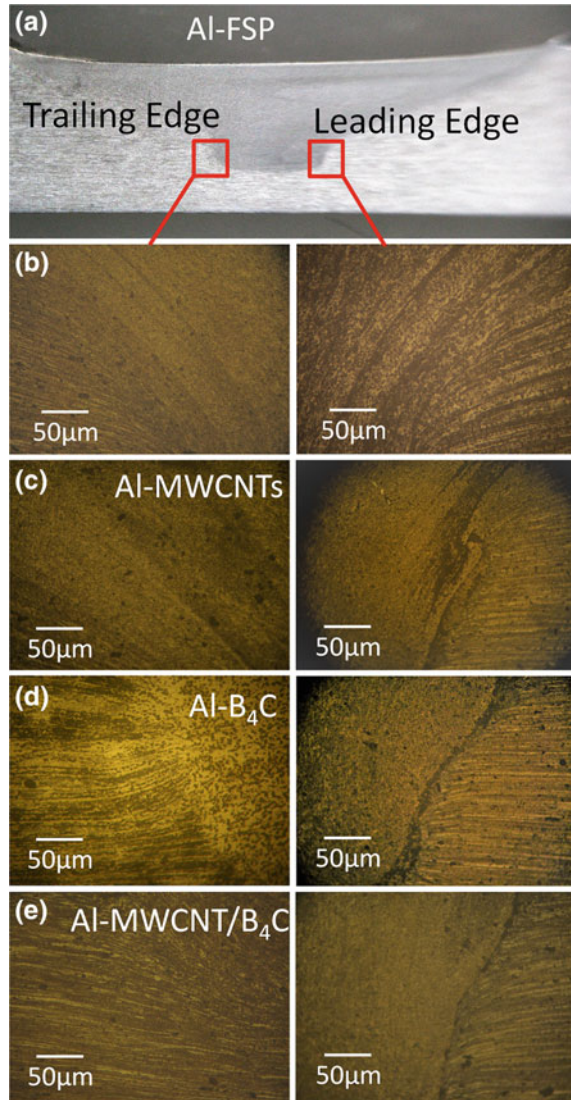
lamellas as a result of the lower volume presence and in responds to the better stirring
action at a single pass.

To perform a detailed optical examination of the FSP reference and composite
samples the microstructural evolution at higher magnification was studied, see Fig. 7.
In Fig. 7a clear transformation line of the grains orientation due to tool stirring can
be seen in the Al-FSP sample, and the MWCNTs clustered in the TMAZ region in
Fig. 7b. As can be seen from Fig. 7b, MWCNT's clustering takes place in lamellae
region which exists between SZ zone and BM zone. The interface strengthening is

Fig. 7 Optical images of:
a reference FSP sample,
b Al-MWCNTs sample,
c Al-B$_4$C sample, and
d Al-MWCNT/B$_4$C sample
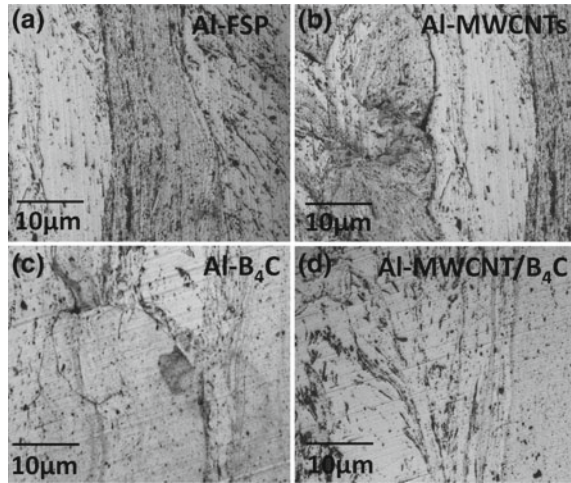
caused by the presence of MWCNTs which are restricted by their diffusion in the BM zone. The microstructure of the Al-B$_4$C composite is characterized by entrapped B$_4$C particles at the interface of the TMAZ region and BM zone, see the blue arrows in Fig. 7c. The hybrid FSP composite Al-MWCNT/B$_4$C and MWCNTs proved to have lower concentration of both reinforcements as compared to the individually reinforced FSP composites. As a result, a lower tendency on clustering, as well as entrapment of B$_4$C particles, was observed, see the red and blue arrows in Fig. 7d.

Hardness Profile

In Fig. 8a the cross sectional harness profile of FSP samples is presented, and in Table 2 the combined mechanical properties of the FSP samples summarized. Moving across from the BM zone to the SZ zone passing through the TMAZ region, noticeable variations in hardness is recorded. Maximum hardness was achieved for Al-B$_4$C composite, i.e. 107 ± 2 HV. Reference FSP sample and Al-MWCNTs composite exhibited minimum values, respectively 91 ± 1 HV and 93 ± 2 HV. However, the hybrid Al-MWCNT/B$_4$C composite revealed an intermediate value of 100 ± 1 HV. Within the FSP sample there is also variations of hardness along the cross sectional zones, which confirms earlier findings by Mahmood et al. [19]. The distinct feature of FSP resulting in grain refinement is obviously the cause of the increase in hardness. It is a well- known fact, that grain refinement originates from tool stirring, causing severe plastic deformation. Grain size reduction is best explained by Hall-Petch equation as referred by Hansen [20]:

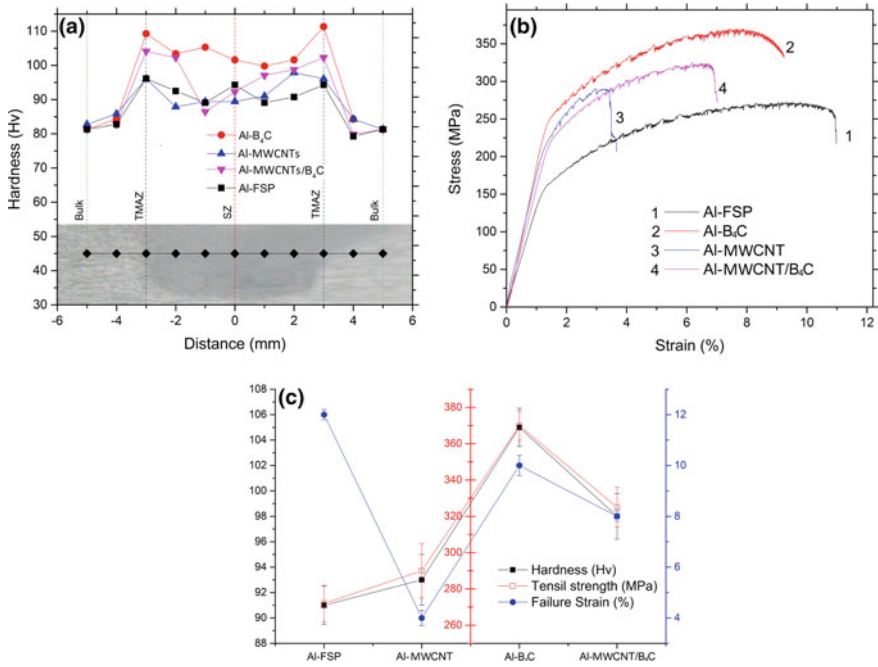$$H_c = H_o + K \cdot D^{-1/2} \qquad (1)$$

Fig. 8 **a** Hardness profile across the FSP cross section in all the samples [15], **b** tensile testing curves of the FSP samples [15], and **c** graph showing mechanical testing data of FSP samples

Table 2 Designations of FSP composites with hardness, and tensile properties

S. no.	Name	Description	Hardness HV	Ultimate tensile strength MPa	Strain (%)
1	Al-FSP	Al5083 FSP reference sample	91 ± 1	272 ± 10	11
3	Al-MWCNTs	Al5083 + MWCNTs FSP composite	93 ± 2	290 ± 15	3.7
5	Al-B$_4$C	Al5083 + B$_4$C FSP composite	107 ± 2	370 ± 8	9.2
7	Al-MWCNT/B$_4$C	Al5083 + MWCNTs/B$_4$C FSP composite	100 ± 1	325 ± 11	7

where; H_c is the hardness of material, grain diameter D. H_o is hardness of the base metal, and K a constant.

The BM zone generally presents the rolled condition as a result of the preliminary grain structure, unless treated otherwise. In contrast to any as received condition of the BM zone, it usually has minimum values of hardness. In present study the interface between SZ zone and BM zone showed highest hardness values. Dislocations pinning and presence of entrapped reinforcements can be attributed as the principle strengthening mechanism. In other words, the severe plastic deformation caused by the tool rotation interlocked the dislocations and they got piled up at the interface restricting further movement, which in turn caused the hardness to increase. TMAZ region exhibited maximum hardness value all FSP samples.

As per results of the microhardness profiling (see Fig. 8a and Table 2), the Al-B_4C composite showed the greatest increase in hardness (~18%). An increase in hardness can be related to the FSP processing and/or the presence of second phase particles. In the case of the Al-MWCNTs composite, an increase in hardness was observed at the interface of the FSP zone confirming the earlier findings of Hosseini et al. [21] and Lim et al. [11]. Even in this case the pinning effect of the dislocation movement is believed to be the reason for the observed increase in hardness. However, the clustering of the MWCNTs composite caused a decrease in hardness in the SZ zone compared to at the interface. The hybrid composite Al-MWCNT/B_4C proved to have the greatest variance in the hardness values, which can be seen in Fig. 8a. Localized synergic effect of dual reinforcement and thermal mismatch of the MWCNTs with B_4C particles is believed to be a possible reason for this severe variance of the hardness in the SZ zone.

Tensile Properties

In Fig. 8b, tensile stress-strain graphs of the different samples is presented, while their tensile properties are plotted in Fig. 8c and summarized in Table 2. As can be seen from the figures and the table, the reference Al-FSP sample shows the ultimate tensile strength of 271 ± 9 MPa with maximum fracture strain of ~11%. It can also be seen that the incorporation of MWCNTs did not significantly enhance the tensile strength value, which was 290 ± 15 MPa but they decreased fracture strain to ~4%. The addition of B_4C particles in the alloy matrix did also result in a significant increase in the tensile strength to 370 ± 10 MPa but with the fracture strain reduced to ~9%. By combining equal amounts of both reinforcements the ultimate tensile strength increased to an appreciable value of 325 ± 11 MPa and a failure strain of ~7%. This value is, however, lower than the value obtained for the FSP composite reinforced only with B_4C particles, and higher than the value obtained when reinforced only with MWCNTs. It has been reported in literature that incorporation of either MWCNTs or B_4C particles to the matrix has shown enhanced tensile strength and comparatively reduced fracture strain. Liu et al. [22] described in their study that strength of material increases with decrease in grain size during dynamic recrystal-

lization. In other words, entrapment of reinforcements at the interface to restrict heat dissipation and elimination of HAZ has also contributed to strengthening the matrix. In a study by Shahraki et al. [23], they discoursed the presence of dislocations due to reinforcements result in pinning and grain size they also concluded that presence of hard particles and grain refinement augments the mechanical behavior of the FSP composite. Another investigation by Guo et al. [24] advocated that Orowan effect is prime reason, responsible for enhanced mechanical properties in FSP composites. However, the clustering of MWCNTs was reported to have deleterious effects on the failure strain at single pass FSP. Du et al. [25] reported that MWCNTs may break down into smaller lengths and disperse into the aluminum matrix inhibiting the dislocation movement, and resulted in a slight increase in strength at cost of the fracture strain, see Fig. 8b.

Base on present results it is believed that the difference in thermal expansion coefficient values of MWCNTs (1.0×10^{-6} K^{-1}), B$_4$C (5.7×10^{-6} K^{-1}) and the matrix, i.e. aluminum: 23.6×10^{-6} K^{-1}, may have produced residual stresses in the final material around the reinforcements, which may have generated dislocations [26]. Dislocation density in matrix depends on the surface area of reinforcement. Thus presence of MWCNTs is expected to produce higher dislocation density which results in increase of strength of final material. The single pass FSP was, however, proven not to be effective in dispersion of nanoreinforcement as compared to the mircosized B$_4$C particles. As a result, the FSP composite with B$_4$C particles have shown greater strength than the composites with MWCNTs, which is in agreement with the results reported by Liu et al. [27]. The premature failure of the FSP composites with MWCNTs can also be related to the clustering of nanoreinforcements. This reduces the effective surface area of MWCNTs and increases the porosity in FSP area.

Fractography

The fractographs of all the FSP samples after tensile test are shown in Fig. 9. Typical ductile fractures corresponding to aluminum and its alloys can be seen for the Al-FSP samples, see Fig. 9a. The inset in the figure presents the higher magnification area for better illustration of the Al-MWCNTs composite. As can be seen from the figure, the Al-MWCNTs composite was observed with cleavage failure dominated by clusters of MWCNTs. These clusters deleteriously damaged the mechanical properties of the final material by presenting lack of fusion defects, as discussed in the radiography section, as shown in Fig. 4b. In the high magnification inset of Fig. 9b, vertically aligned MWCNTs are seen from the region marked by red. The bridging effect, earlier reported by Deng et al. [28], is believed to be related to the slight increase observed in the ultimate tensile strength of the FSP composite, as well as the premature failure headed by the MWCNTs clustering. The clustering in the Al5083 matrix enables the metal to slide over to fail the composite at low strain values. The single pass FSP stirring action is also believed to be a possible reason for insufficient distribution

Fig. 9 SEM fractographs of FSP specimens after tensile test: **a** reference FSP sample, **b** Al-MWCNTs, **c** Al-B$_4$C and **d** M-MWCNT/B$_4$C
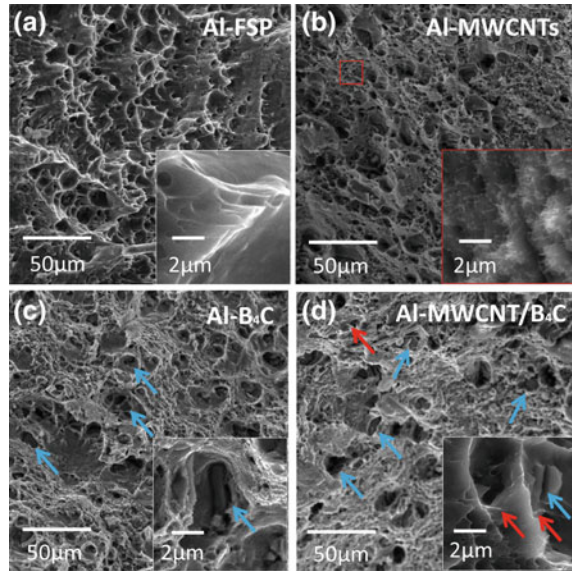
of MWCNTs in the Al5083 matrix. The FSP composite incorporating B$_4$C particles showed, however, uniform distribution of reinforcement and the fracture surface showed micro-cracks initiated by the ceramic reinforcement/matrix interface, see the blue arrow in Fig. 9c. The B$_4$C particles are seen surrounded with matrix alloy dimples, which is visualized as deep wells, due to the peening effect. Uniform distribution of B4C is believed to be the main reason for obtaining the highest strength in the FSP composites tested. The hybrid FSP composite with MWCNTs and B$_4$C particles, showed MWCNTs bridging at the crack tips, as shown with red arrow in Fig. 9c, and at wells of ceramic B$_4$C. The intermediate mechanical properties of the FSP hybrid composite indicated the dominance of micro sized ceramic reinforcement in comparison to the poor distribution of the nano-scale MWCNTs single pass FSPs. It should in this context be mentioned that synergic behavior was not prominent at the presently selected processing parameters.

Bend-Ductility Test

The Al-FSP reference sample presented in Fig. 10a proved to have the maximum fracture strain of all the materials tested (see Table 2). The same was found in regards to the bend ductility test, which revealed the maximum cold formability. The curved surface of reference FSP specimen showed no evidence of any cracking by the naked eye nor under microscopic examination on either sides of the sample, as shown in Fig. 10b, c. The bend-ductility samples with MWCNTs, see Fig. 10d, was possible
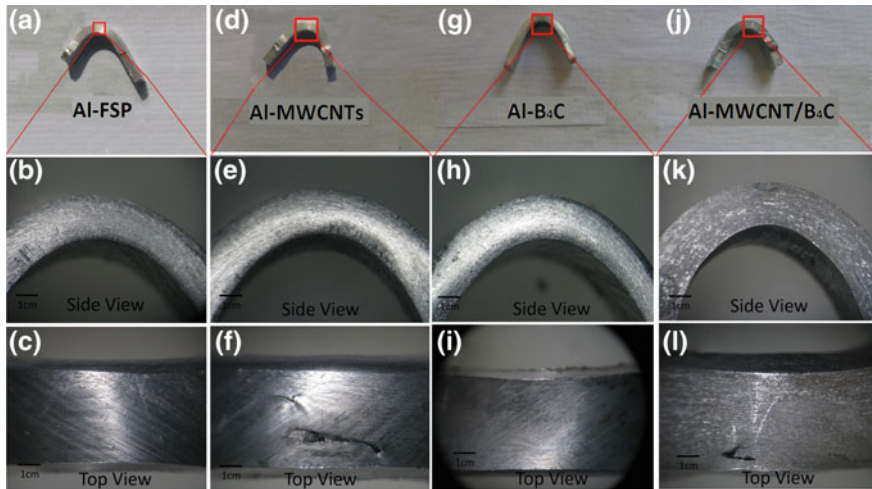
Fig. 10 Images of the side and top view of the bend-ductility samples; **a–c** reference Al-FSP samples **d–f** Al-MWCNTs samples, **g–i** Al-B$_4$C samples, and **k–i** hybrid Al-MWCNT/B$_4$C composite samples [15]

to bend up to full limits of the die, but distinct cracks were obtained alongside the SZ zone starting from the TMAZ region resulting in a cracked surface, see Fig. 10f. No visible evidences of any cracks appeared on either sides and convex surface of the B$_4$C containing FSP sample, see Fig. 10d–f, nor on the side of the hybrid FSP composite specimen, as shown in Fig. 10j, k. However, a ~12 mm crack surface appeared was observed on top view of the hybrid FSP composite specimen, as shown in Fig. 10i.

The overall results of the bend-ductility tests showed that the cold formability of the FSP samples corresponded to the cracking regardless of the mechanical strength. Among the four FSP samples tested in the present study only the Al-MWCNTs composite and the hybrid composite showed cracking in the bend area curvature under tensile stresses. The maximum recorded fracture strain of the FSP reference sample can be related to the maximum formability exhibited during the bend-ductility tests. Similarly, no cracking appeared on the surfaces of FSP composite with B$_4$C particles, and its failure strain was recorded as the second highest to reference the FSP sample. It is believed that the FSP composite with MWCNTs could not survive bend test and failed due to: (a) clustering of the MWCNTs near the TMAZ region, (b) poor mechanical bonding with the alloy matrix, and (c) retention of voids/porosity generated due to drilled holes for incorporating the MWCNTs in the base plate. The second FSP composite to fail in bend test was hybrid Al-MWCNT/B$_4$C composite, where cracks appeared on convex side of the sample, as shown in Fig. 10l. Unlike the fracture in the MWCNTs FSP composite, the length of crack was ~1/5th in the case of the hybrid composite. The behavior of the MWCNTs to cluster at single pass FSP seems to dominate the cold formability in the alloy matrix. However, the B$_4$C

particles restricted the crack propagation as a result of second phase strengthening which is evident from the fracture strain values obtained (~7%).

Conclusions

FSP is among emerging versatile surface modification techniques to yield promising properties in aluminum matrix composites. In the present study cold formability was determined for FSP composites with reference, individually and hybrid reinforcements, and microstructure evolution was studied using optical and SEM. Increase in average hardness was recorded for all the FSP composites with a maximum of ~18% for B_4C reinforced composite samples. Tensile test was carried out to determine effects of processing on mechanical properties of the FSP reference and composite samples. An improvement in ultimate tensile strength of ~36% at the cost of ~3% failure strain was recorded for the B_4C reinforced FSP composite samples. In the case of the Al-MWCNTs composite clusters was identified due to an uneven distribution in the alloy matrix resulting in inferior mechanical properties. Composite containing MWCNTs showed minimum fracture strain (3.7%) while its hardness and tensile strength values were comparable to the reference FSP sample. Additionally, it failed in bend test as cracks appeared on curved surface. Hybrid Al-MWCNT/B_4C samples showed comparatively higher tensile strength, hardness and fracture strain than MWCNTs composite samples. Poor MWCNTs distribution and weak interfacial MWCNT/Al bonding are concluded to be the possible reasons. Multiple-pass friction stir processing can be employed to enhance MWCNTs distribution. Based on the bend-ductility test of the Al5083 single pass FSP composites, an approximate threshold of ~8% failure strain in the tensile test can be proposed for cold formability without cracking.

References

1. Mishra RS, Ma ZY (2005) Materials science and engineering: R. Reports 2005, vol 50, pp 1–78
2. Nascimento F, Santos T, Vilaga P, Miranda RM, Quintino L (2009) Mater Sci Eng A 506:16–22
3. Khan M, Rehman A, Aziz T, Naveed K, Ahmad I, Subhani T (2017) Mater Sci Eng A 696:552–557
4. Guru PR, Khan Md F, Panigrahi SK, Janaki Ram GD (2015) J Manufact Process 18:67–74
5. Maurya R, Kumar B, Ariharan S, Ramkumar J, Kantesh B (2016) Mater Design 98:155–166
6. Joyson Abraham S, Chandra Rao Madane S, Dinaharan I, John Baruch L (2016) J Asian Ceramic Soc 4:381–389

7. Wang W, Shi Q-Y, Liu P, Li HK, Li T (2009) J Mater Process Technol 209:2099–2103
8. Azizieh M, Kokabi AH, Abachi P (2011) Mater Des 32:2034–2041
9. Srinivasu R, Sambasiva Rao A, Madhusudhan Reddy G, Srinivasa Rao K (2014) Defence Technol
10. Hosseini SA, Ranjbar K, Dehmolaei R, Amirani AR (2015) J Alloys Comp 622:725–733
11. Lim DK, Shibayanagi T, Gerlich AP (2009) Mater Sci Eng, A 507:194–199
12. Jeon CH, Jeong YH, Seo JJ, Tien HN, Hong ST, Yum YJ, Hur SH, Lee KJ (2014) Int J Precision Eng Manufact 15:1235–1239
13. Suri AK, Subramanian C, Sonber JK, Ch Murthy TSR (2010) Int Mater Rev 55:4–40
14. Salvetat J-P, Bonard J-M, Thomson NH, Kulik AJ, Forro L, Benoit W, Zuppiroli L (1999) Appl Phys A 69:255–260
15. Khan M, Rehman A, Aziz T, Shahzad M, Naveed K, Subhani T (2018) J Mater Process Technol 253:72–85
16. McNelley TR (2010) Revista de metalurgia 46:149–156
17. Lee IS, Hsu CJ, Chen CF, Ho NJ, Kao PW (2011) Composites Sci Technol 71:693–698
18. Taban E, Kaluc E (2007) Kovove Mater 45:241
19. Mahmoud ERI, Ikeuchi K, Takahashi M (2008) Sci Technol Weld Joining 13:607–618
20. Hansen N (2004) Scripta Mater 51:801–806
21. Hosseini SA, Ranjbar K, Dehmolaei R, Amirani AR (2015) J Alloys Compounds 622:725–733
22. Liu Q, Ke L, Liu F, Huang C, Xing L (2013) Mater Des 45:343–348
23. Shahraki S, Khorasani S, Behnagh RA, Fotouhi Y, Bisadi H (2013) Metallurg Mater Trans B 44:1546–1553
24. Guo JF, Liu J, Sun CN, Maleksaeedi S, Bi G, Tan MJ, Wei J (2014) Mater Sci Eng A 602:143–149
25. Du Z, Tan MJ, Guo JF, Bi G, Wei J (2016) Mater Sci Eng A 667:125–131
26. George R, Kashyap KT, Rahul R, Yamdagni S (2005) Scripta Mater 53:1159–1163
27. Liu ZY, Xiao BL, Wang WG, Ma ZY (2014) Carbon 69:264–274
28. Deng C, Zhang X, Wang D, Lin Q, Li A (2007) Mater Lett 61:1725–1728